Taylor & Francis
Taylor & Francis Group

Modeling of Electrical Crosstalk in OEIC Modules

DIMITRIS VAROUTAS
AGGELIKI ARAPOYIANNI
THOMAS SPHICOPOULOS

Department of Informatics and Telecommunications
University of Athens
Panepistimiopolis, Ilissia, Athens 15784, Greece

A complete set of tools for the calculation of electrical crosstalk in optoelectronic integrated circuits is presented. Typical chip architecture has been analyzed and relative results are obtained. The model can be easily applied to several wire-bonded and flip-chip OEICs. Design guidelines are presented and discussed.

Introduction

During recent years, the monolithic integration of photonic devices into a single chip has attracted considerable interest from many research groups worldwide [1]. Different types of integrated modules—known as photonic integrated circuits (PICs) or optoelectronic integrated circuits (OEICs)—have been proposed with the potential of giving a considerable boost to the performance of existing or proposed advanced photonic systems, due to their attractive options for the monolithic integration of optical amplifiers and wavelength converters on the chip [2–4]. In addition, optoelectronic VLSI (OE-VLSI) technology provides close integration of photonic devices with VLSI electronics [5].

The goal is to design these modules at low cost together with high fabrication yield while satisfying the required specifications, which are to supply multiple high-performance optical inputs and outputs with aggregate data rates up to Tbps. However, as these modules are miniaturized for reasons of cost reduction as well as improved compactness and functionality, a significant increase in undesired interactions between their individual building blocks and elements, and consequently between the transmission and the receiving channels, is expected [6–12].

One of the most critical parameters in the module design and its functional optimization is the crosstalk between the laser and the photodiode. It consists of contributions of electrical origin (leakage and induction currents, parasitic capacitance and inductance) as well as optical origin (scattered light, back reflections, etc.) [8, 9]. In most cases, the distinction between these two different sources of crosstalk is difficult, and consequently, one single figure is specified for the overall crosstalk.

This article describes the electrical crosstalk problem in OEIC modules and introduces convenient lumped models for its estimation of the electrical crosstalk through the analysis of different crosstalk sources and their contribution to the overall module performance.

Electrical Crosstalk Problems in OEIC Modules

The importance of crosstalk can be revealed by considering the difference between the laser diode drive current (order of 100 mA) and the photocurrent (order of 100 nA), which is of 6 orders of magnitude. In addition, the optical power emitted from the laser is of the order of 1 mW, whereas the power incident to the photodiode is of the order of 100 nW, implying a difference of 4 orders of magnitude.

For the design of the early transceiver modules, a hybrid approach was adopted where the laser and the photodiode were physically separated. The advantages of this approach were the elimination of the electrical crosstalk and the considerable reduction in the design complexity. The disadvantage was the increased cost related to the module assembly. In most cases the module was formed by hybridly combining two OEIC chips, one for the laser and the wavelength duplexer and another for the photodiode.

Later approaches were focused on the monolithical integration of these subcomponents into an OEIC [9–11]. The main challenge is the implementation of the complete Tx/Rx function within one chip attaining at the same time to sufficiently suppress both the electrical and the optical crosstalk between the integrated laser and the photodiode. Depending on the system applications, the optical crosstalk suppression ratio must be from 28 dB up to more than 45 dB. Equivalent performance has to be achieved for the electrical crosstalk suppression ratio on the whole module setup.

In order to achieve these requirements, different approaches can be adopted:

- Application of a dual stage optical filter principle;
- Adoption of absorber bars in order to absorb straylight coming from the integrated laser transmitter;
- Maximization of the on-chip distance between the laser and the photodiodes in order to eliminate capacitive coupling between pn-junctions and leakage currents;
- Utilization of the semi-insulating substrate and waveguide material to avoid leakage currents and parasitic capacitances within the chip.

By adopting these techniques the optical crosstalk can be significantly suppressed (a typical value is about −40 dB) while the electrical crosstalk, being very sensitive to the specific design characteristics of the module, can reach values up to −10 dB at high bit rates, raising additional limitations for high-speed systems. Recent developments on hybrid flip-chip bonded optoelectronic technology have shown many advantages in comparison to standard wire-bonded optoelectronic packaging due to minimization of electrical parasitics (bondwire inductance, pads capacitance, etc.) [5, 12].

The problem of the electrical crosstalk in OEIC modules can be attributed mainly to three major sources: the crosstalk between laser and photodiodes through the common substrate, the bondwire coupling, and the coupling between microstrip lines. Therefore, in order to analyze the whole crosstalk performance of an OEIC module, a procedure that takes into account all crosstalk sources in a convenient and similar way must be adopted.

In this article such a procedure based on lumped models is introduced. Equivalent capacitance, resistance, and inductance lumped models for the three main contributions to

the overall electrical crosstalk (due to microstrip, bondwire, and substrate coupling) are represented. The appropriate equivalent circuits describing the laser and the photodiodes have been introduced.

Several methods can be used to determine the element values of the basic elements of any OEIC module. The methods used in this work can be summarized in the following:

- For the inductive coupling of the bondwires, the method used is based on the calculation of mutual inductance of bondwires by solving the Newman potential equation.
- For the capacitive coupling of the bondwires, the calculation of capacitive matrices is based on the integral form of Laplace's equations using Green functions. The equations have been solved using the Methods of Moments.
- For the substrate resistive coupling, an electrostatic approach has been adopted and the electrical crosstalk is estimated by a Finite Elements Method.
- For microstrips, analytical expressions for capacitances have been adopted.
- Finally, the equivalent circuits of laser and photodiode are integrated in the model, providing a complete electrical crosstalk model.

These methods have been optimized or developed and the resulting electrical parameters of the equivalent circuit have been used for the analysis of the whole OEIC module using an electrical simulation program, (i.e., SPICE) in order to calculate the overall crosstalk performance.

Definition of Crosstalk

The calculated crosstalk refers to coupling of the modulated signal of the laser with the current induced to the photodiode. This coupling is usually measured in decibels and it's given by:

$$\text{Crosstalk}_{\text{dB}} = 20 \log \left(\frac{I_c}{I_{PD}} \right) \tag{1}$$

where I_c is the current induced to the photodiode due to all kinds of parasitic coupling and I_{PD} is the photodiode current. Alternatively, the term "isolation" can be used, which is given by:

$$\text{Isolation}_{\text{dB}} = 20 \log \left(\frac{I_c}{I_{LD}} \right) \tag{2}$$

where I_{LD} is the laser drive current. In many cases, this feature can be easily extracted from a simulation program, since it's related to the AC analysis of the circuit.

In general, the crosstalk and the isolation are related by:

$$\text{Crosstalk}_{\text{dB}} = \text{Isolation}_{\text{dB}} + 20 \log \left(\frac{I_{LD}}{R \cdot P_{PD}} \right) \tag{3}$$

where R is the photodiode's responsivity and P_{PD} is the incident power to the photodiode.

The module analyzed in this work includes a ridge waveguide DFB laser, a router network (duplexer), and a "wavelength selective" photodetector (WSP) as basic building blocks (Figure 1) [9]. The WSP is a key component for suppression of optical crosstalk and, in combination with the router, guarantees the demanded performance. Light baffles
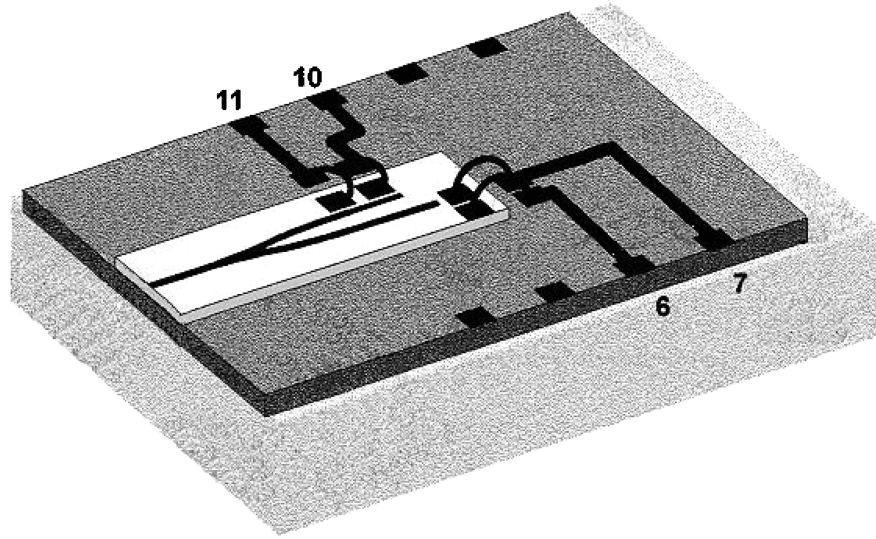
Figure 1. Typical wire-bonded 1.3/1.5 OEIC module.

are used for not-guided laser straylight. Moreover, using a semi-insulating substrate, waveguide material to avoid leakage currents, and parasitic capacities within the chip and a sufficient on-chip LD/PD distance, the electrical crosstalk is minimized. Detailed information concerning the analyzed OEIC module is presented in Table 1.

Thus, for $I_{LD} = 100$ mA, photodiode's responsivity $R = 0.7$ A/W, and power incident $P_{PD} = 100$ nW, the crosstalk and the isolation are related by:

$$\text{Crosstalk}_{dB} = \text{Isolation}_{dB} + 123 \text{ dB} \tag{4}$$

Electrical Analysis of Elements Used in the Crosstalk Model

Electrical Model of the Laser Diode

Several electrical circuit models for the laser operation have been proposed, based on the transmission line method [16] and the lumped-element method [13–16]. The lumped-element-based models 16 are "one-level" models since the rate equations used describe only the interaction between the bound states of the QW and the photon population. Several models [12, 16] are based on "two-level" rate equations for the representation of the carrier dynamics within the laser. One equation describes the continuity of carrier charge in the QW, while the other performs the same function for carriers in the separate-confinement heterostructure (SCH). Carriers are considered able to exchange directly between the continuum states of the SCH and the bound states of the QW.

The most recent "two-level" models [12, 16] incorporate in the description of carrier interchange an exit flow of carriers from the SCH at the SCH/QW boundary. The phenomenon of carrier transport within the SCH has a significant effect on the high-speed properties of QW lasers.

The model proposed in [18] is based on the three-level rate equations and includes characterization of charge dynamics and the role of gateway states at the QW. This model

Table 1
Typical values for a wire-bonded OEIC

Chip thickness	350 μm
Chip size	2.0 μm $\times$ 0.5 μm
Substrate thickness	640 μm
Substrate dielectric constant ε_r	$\sim$9.2
Substrate resistivity	10^7 Mohm $\times$ cm
Microstrip width	60 μm
Microstrip separation	2.54 mm
Bondwire diameter	40 μm
Bondwire separation	150 μm
Bondwire length	$\sim$1300 μm
Pads dimensions	60 μm $\times$ 60 μm
Laser dimensions	100 μm $\times$ 300 μm
Laser threshold current (max)	25 mA
Laster operation current	100 mA
Laser operation current (max)	150 mA
Laser modulation current	1.5 mA
Photodiode dimensions	10 μm $\times$ 50 μm
Photodiode dark current	<0.1 μA
Photodiode responsivity	0.7 A/W
Laser-photodiode distance	1000 μm

allows both small- and large-signal simulations and, therefore, both frequency response of the OEIC and turn-on delay calculations can be performed.

Since the presented analysis is mainly focused on the influence of the electrical crosstalk to the whole OEIC performance, a simplified model for the laser source has been used based on [15]. A more improved model of the laser could be easily included in this analysis since it is modular.

The following equations provide the LD electrical circuit elements used in this analysis.

$$R = R_d \frac{I_{th}}{I_0} \tag{5}$$

$$L = \frac{R_d \tau_{ph}}{\left[\dfrac{I_{th}}{I_0} - 1\right]} \tag{6}$$

$$C = \frac{\tau_s}{R_d} \tag{7}$$

where $R_d = 2kT/qI_d$ is the usual expression for the differential resistance of the diode, k is the Boltzmann's constant, T is the absolute temperature of the material, q is the electron charge, τ_s is the spontaneous carrier lifetime, τ_{ph} is the photon lifetime, I_o is the bias current of the laser diode, and I_d is approximately equal to the laser current below threshold and to the threshold current for currents above threshold.
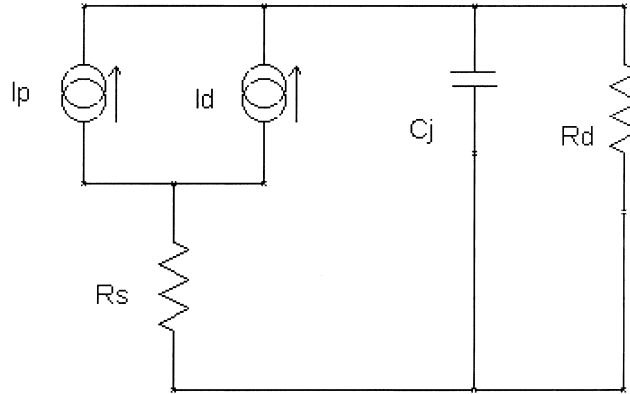
Figure 2. Equivalent circuit for a discrete p-i-n diode.

For the module analyzed in this work, from equations (5)–(7) the following typical parameters have been calculated: $R = 10$ Ohms, C is between 1 and 5 pF, and L is of order of pH.

Electrical Analysis of the Photodiode

The equivalent circuit of a photodiode [19–21] is shown in Figure 2. The diode contains a photocurrent source $I_p(t)$, a dark current source I_d, a depletion capacitance C_j, a series conductance $1/R_s$, and a shunt conductance $g_d = 1/R_d$. For a properly fabricated receiver p-i-n the shunt conductance is negligible with respect to the external circuit conductance.

The series resistance, usually less than 10 Ω, corresponds to the ohmic drop through the undepleted epitaxial layer and the substrate. The junction capacitance is given by:

$$C_j = \frac{\Gamma \varepsilon_s A}{W} \tag{8}$$

where ε_s is the permittivity of the depleted semiconductor, A is the junction area, W is the depletion depth, and Γ is a geometric factor slightly greater than one, which accounts for the deviation of the junction from the parallel plate geometry.

For p-i-n photodiodes R_s has typical values of about 1 Ω and C_j is of the order of tens of pF. Since the shunt resistance is between 10^7 and 10^{11} ohms, the resistive terms can be neglected over a wide range of applications [20]. So only the junction capacitance must be taken into account. A typical value is about 5–20 pF.

Resistive Coupling through the Substrate

The coupling estimation between laser and photodiode through the common substrate is based on electrostatic analysis by using a finite elements method (FEM). Basically this is a three-dimensional problem, since the relative orientation of the devices is important. In a first approach, a two-dimensional analysis can be adopted and fairly reliable results can be promptly available in a simple way.

The first step of the analysis is to find the electrical characteristics of the laser and the photodiode, which provide the appropriate boundary conditions in the FEM analysis
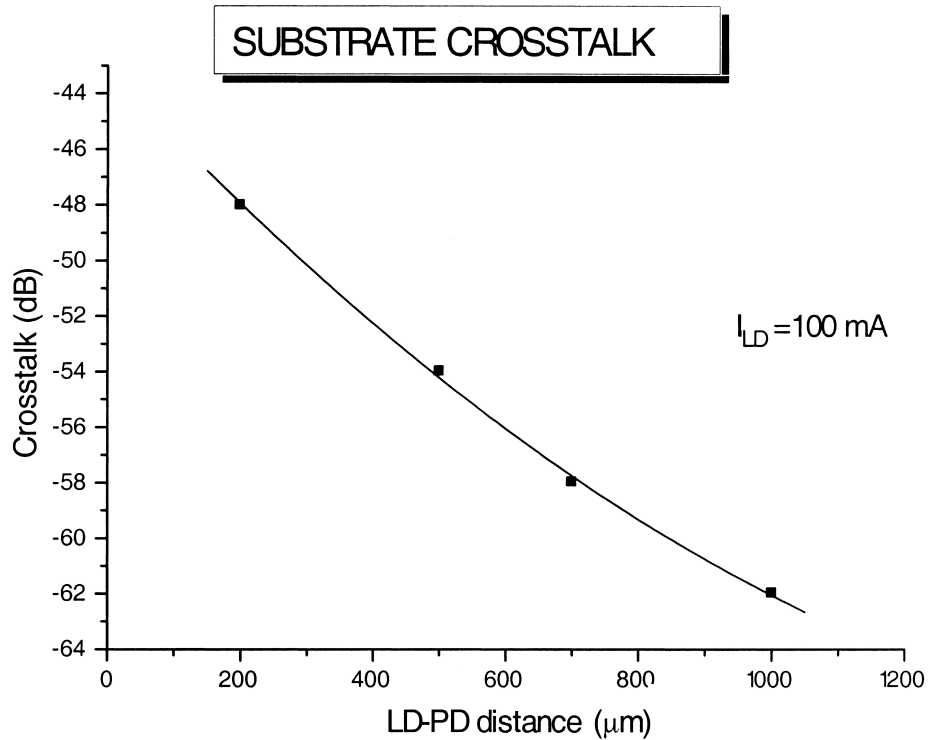
Figure 3. Crosstalk due to the coupling LD-PD as a function of distance between LD-PD.

of the OEIC and therefore the potential and electrical field distributions within the whole structure are computed. This is carried out by applying a current to the laser (as a current boundary condition) and taking into account the ground planes and the electrodes' voltages (as a voltage boundary condition). The dark current of the photodiode can be neglected.

In the second step, the current and voltage distributions in the laser and photodiode bottom are used as boundary conditions for the calculation of the voltage and current distributions within the substrate. In this way, the actual structure (laser and photodiode layers, substrate) of the OEIC are taken into account and the equivalent coupling resistance is calculated.

Using an FEM for a typical transceiver module (Figure 1), it was observed that the potential has been already practically annihilated very close to the laser, while the photodiode is 1 mm away (Figure 3). This means that for this specific structure, the crosstalk attributed to the common substrate is negligible due to the semi-insulating substrate.

Furthermore, it must be noted that the crosstalk due to capacitive coupling through the common substrate is also negligible for the same reason [22].

Bondwire Coupling

Capacitive Coupling of Bondwires. The effect of parasitic bondwire coupling must be included in the full circuit analysis of an OEIC chip in order to have a correct estimation

of the electrical crosstalk [23]. The capacitance matrices of the bondwire layout can describe this kind of coupling. Since the dimensions are much smaller than the wavelength of operation, a static approximation is sufficiently correct and can be applied.

In order to calculate the capacitance matrix of a set of N_c bondwires of arbitrary geometry and orientation in space, a method based on integral form of Laplace's equation using space domain Green's function has been adopted. The equation is solved by the Method of Moments [24] in order to calculate the charge density on the bondwires.

Since the bondwires' radii are very small compared to their length, we assume that the charge density distribution is directed along their axis and can be approximated by:

$$\rho_i(x_i, y_i, z_i) = \delta(x_i) f(y_i)\delta(z_i) \qquad i = 1, \ldots, N_c, \tag{9}$$

where (x_i, y_i, z_i) are orthogonal coordinate systems adjoint to each bondwire with y-axis colinear to their axis, $f(y)$ is the charge distribution function, and $\delta(\cdot)$ is the delta function. In the above, all conductors are assumed to be perfect, so ohmic losses are not included in our analysis. The evaluation of the elements of this matrix stems from the static integral equation:

$$\Phi(\bar{r}) = \int_V G(\bar{r}, \bar{r}'_i) -_i (\bar{r}'_i)d\bar{r}'_i \qquad i = 1, \ldots, N_c \tag{10}$$

The above equation relates the electrostatic potential $\Phi(\bar{r})$ to the charge density, $\rho(\bar{r})$, $G(\bar{r}, \bar{r}')$ is the Green's function of the problem, while the volume integral of equation (10) includes all the charges. The capacitance matrix can be computed by solving equation (10) with respect to the charge density with various settings of voltages on the conductors.

The Green's function corresponds physically to the potential created by unit point sources and depends only on the source–observer distance $|\bar{r} - \bar{r}'_i|$. In this problem, the static Green's function describes a dielectric layer over an ideal ground plane and the conductor is assumed to be embedded in a single layer with dielectric constant ε_r.

$$G(\bar{r}, \bar{r}') = \frac{(1 - \varepsilon)}{4\pi\varepsilon_0} \left[\frac{1}{R_0} - (1 + \varepsilon) \sum_{n=1}^{\infty} (-\varepsilon)^{n-1} \frac{1}{R_n} \right] \tag{11}$$

where $R_n = \sqrt{(x - x'_i)^2 + (y - y'_i)^2 + (z - z'_i)^2 + 4n^2h^2}$, and $\varepsilon = (\varepsilon_r - 1)/(\varepsilon_r + 1)$.

The series in equation (11) is the well-known partial image representation of the static Green's function. Since the potentials on the bondwires are given, equation (10) has to be solved in order to compute the associated charge distribution. The Method of Moments can do this efficiently.

In the following, each bondwire is described by a linearized wire model of three linear segments (Figure 4). So, the initial system of N_c bondwires is equivalent to $M = 3N_c$ linear segments. Consequently, the Method of Moments is applied, by discretizing the length of each linear segment with N_i equal subsections (cells) $i = 1, \ldots, M$, where i specifies each linear segment of length l_i and subsection length S_i. The subsection lengths are not necessarily equal for all segments. Then, the unknown charge density can be expanded in a linear basis of triangular functions of the form:

$$f_k(y) = \begin{cases} \dfrac{S_k}{D_k(y)} + \dfrac{y}{D_k(y)} & -S_k < y < S_k \\ 0 & \text{elsewhere} \end{cases} \tag{12}$$
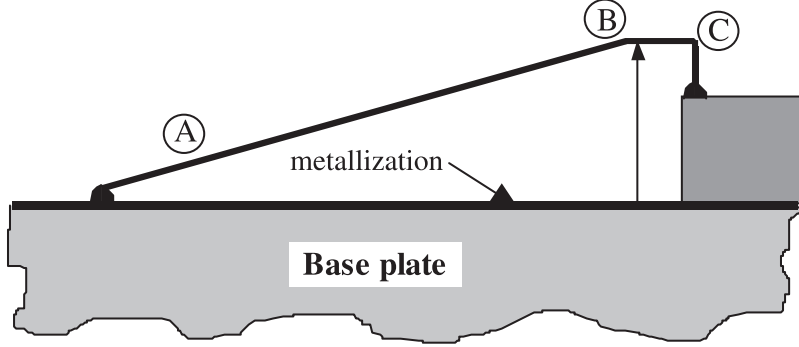
Figure 4. Straight-line wire segment approximation of bondwire.

$k = 1, \ldots, N_{\text{TOT}}$, and $N_{\text{TOT}} = N_1 + N_2 + \ldots$, is the total number of cells. $D_k = \sqrt{y - (l_k - y)}$, l_k is the length of each linear segment, and $D_k = D_i$ for $\sum_{i=1}^{i} N_{i-1} \leq k < \sum_{i=1}^{i+1} N_{i-1}$, $i = 1, \ldots, M$, $N_0 = 1$. The denominator has a singular behavior in the neighborhood of the linear segment edges, in order to take into account the real behavior of charges in the electron's edges and depends on the reference bondwire. Consequently, the unknown charge density along each linear segment can be expressed in its associated orthogonal axis system as:

$$\rho_i(y) = \sum_{k=1}^{N_{\text{TOT}}} q_k f_k(y_k) \qquad i = 1, \ldots, M \tag{13}$$

where q_k are unknown coefficients. Then, by applying the point matching technique, that is by enforcing equation (10) to be satisfied at each subsection center $\bar{r}_j$, $j = 1, \ldots, N_{\text{TOT}}$, the integral equation is discretized and translated into an $N_{\text{TOT}} \times N_{\text{TOT}}$ square matrix form:

$$V_j = \sum_{k=1}^{N_{\text{TOT}}} q_k \int_{-S_k}^{S_k} G(\bar{r}_j - \bar{r}'_k) f_k(y'_k) dy'_k \tag{14}$$

V_j is the voltage difference between the jth linear segment where the cell j is belonging and the ground plane and is defined by the initial conditions. Solving the $N_{\text{TOT}} \times N_{\text{TOT}}$ linear system (equation [13]) the unknown coefficients q_k are determined. Once the charge distribution on each bondwire is available, the corresponding total charge Q_{TOT} can be computed since the capacitance matrix is associated to the total charge and the potential of each bondwire through the well-known equation

$$Q_i^{\text{TOT}} = \sum_{j=1}^{N_i} C_{ij} V_j \qquad i = 1, \ldots, N_c, \quad j = 1, \ldots, N_c \tag{15}$$

Each element C_{ij} is evaluated by setting $V_j = \delta_{ji}$, where δ_{ji} is the Kronecker's symbol. The so-calculated capacitance matrix of the bondwires system is a measure of the expected crosstalk and is to be included to the equivalent circuit representation of the OEIC module.

Inductive Coupling of Bondwires. In order to calculate the inductive behavior of the bondwires, a simple and accurate method valid up to several GHz has been incorporated in the model.

The approach is based on magnetostatic analysis and the related formula for the mutual inductance is given by:

$$M = \frac{\mu}{4\pi} \oint_{C_2} \oint_{C_1} \frac{d\vec{l}_2 d\vec{l}_1}{|r_2 - r_1|} \tag{16}$$

where μ is the permeability and r_i is the distance of the ith segment of length dl_i from the beginning of the axes (Figure 5).

For rectilinear wires, equation (15) can be written in the following form:

$$M = \frac{\mu}{4\pi} \iint \frac{ds_1 ds_2}{r_{12}} \tag{17}$$

where r_{12} denotes the distance between the two segments with ds_1 and ds_2 lengths. This formula is also known as "Newman's potential" and represents the portion of magnetic energy arising from the interaction of the two circuits.

In this kind of analysis, the term "mutual inductance per unit length" cannot be introduced, since mutual inductance is not proportional directly to the length l. The reason is that two closed circuits are calculated rather than two circuit segments. This is obvious in the case of two parallel wires of equal length, in which the above formula leads to:

$$M = \frac{\mu}{2\pi} l \left(\log \frac{2l}{\alpha} - 1 \right) \tag{18}$$

where l is the length of the wires and α is the distance between the wires. But this formula can be applied also in the case of linear parts in non-rectilinear circuits segments. In this case, the total inductance will be the superposition of each part's inductance. In Figure 4, the straight-line wire segment approximation of bondwire used for the calculations is illustrated.

In Figure 6, the exponential behavior of the mutual inductance as a function of the electrode's length is presented. The mutual inductance actually depends on the length of the shorter electrode since this indicates the interaction "length" for the magnetic field. For $L_1 = 1$ mm and $L_2 > 1$ mm, the mutual inductance varies very little with the second electrode length.
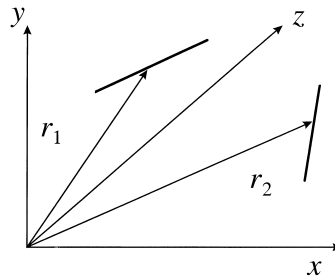

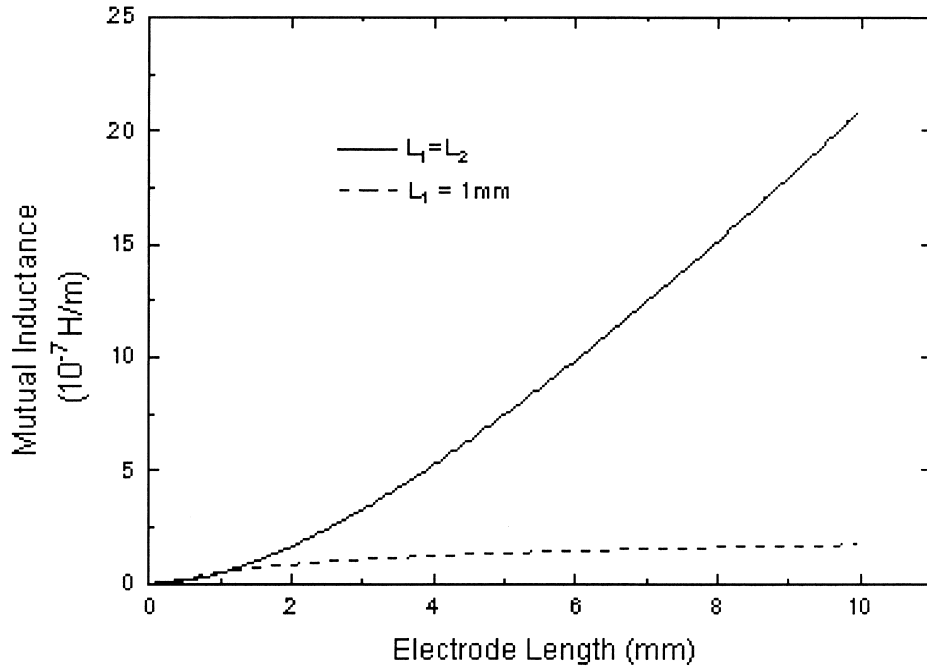**Figure 5.** General geometry for two arbitrarily oriented bondwires.

Figure 6. Mutual inductance as a function of electrode length.

In the case of two pairs of bondwires, the total self-inductance of each pair of bondwire can be calculated by the following formula:

$$L_s = \sum L_{ii} - \sum_{i \neq j} L_{ij} \qquad i, j = 1, 2 \tag{19}$$

where L_{ii} is the self-inductance of ith bondwire and L_{ij} is the mutual inductance of the bondwires. The self-inductance of each bondwire is given by the following equation:

$$L_{ii} = \frac{\mu}{2\pi} l_i \left(\log \frac{2l_i}{b_i} - \frac{3}{4} \right) \tag{20}$$

where l_i is the length of ith bondwire and b_i is its radius.

Thus, a total self-inductance (or operating inductance) of each pair of bondwires can be extracted. In the case of identical bondwires the above equation leads to:

$$L_s = 2(L_{ii} - M) \qquad \text{for } i = 1, 2, \text{ or } 3, 4 \tag{21}$$

The mutual inductance between two pairs of bondwires must be calculated separately and a total mutual inductance must be included in the equivalent circuit. If the feeding electrodes are the electrodes 1 and 3 (or 2 and 4) then the mutual inductance is given by:

$$M = L_{13} + L_{24} - L_{23} - L_{14} \tag{22}$$

With the above-described equations the equivalent circuit can be simplified and the inductive coupling can be easily included in the calculations.

Analysis of Crosstalk through Microstrip Lines

Due to the lumped approach of the whole model, a lumped model for coupled microstrip lines and discontinuities has been incorporated. Although characteristics of uniform coupled lines have been studied extensively [25], used widely, and are accurate enough for crosstalk calculations, discontinuities and bends must be taken into account for a more generic model.

The model used and proposed by this work has been introduced by [26] and is a combination of two-dimensional planar and lumped-element networks. For coupling between microstrips the capacitance and inductance matrices are given by:

$$[C] = \begin{bmatrix} C_{11} & C_{12} \\ C_{21} & C_{22} \end{bmatrix} = \begin{bmatrix} \dfrac{(C_e + C_o)}{2} & \dfrac{(C_e - C_o)}{2} \\ \dfrac{(C_e - C_o)}{2} & \dfrac{(C_e + C_o)}{2} \end{bmatrix} \tag{23}$$

and

$$[L] = \begin{bmatrix} L_{11} & L_{12} \\ L_{21} & L_{22} \end{bmatrix} = \mu_o \varepsilon_o [C]^{-1} \left[\frac{\text{Henry}}{m} \right] \tag{24}$$

where C_e and C_o are even and odd capacitances, respectively, and, given by [27]:

$$C_0 = \varepsilon_0 K(k')/K(k) \tag{25}$$

with $k = s/d$, $k' = \sqrt{1 - k^2}$, s the distance between the inside edges of the conductors, d the distance between the outside edges of conductors to the outside edge of the other conductor, and K the complete elliptic integral of the first kind and:

$$C_\varepsilon = \varepsilon_0(\varepsilon_r + 1)K(k_1')/K(k_1) \tag{26}$$

where $k_1 = \tanh(\pi s/4h)/\tanh(\pi d/4h)$, $k_1' = \sqrt{1 - k_1^2}$, and h is the finite substrate thickness (Figure 7).
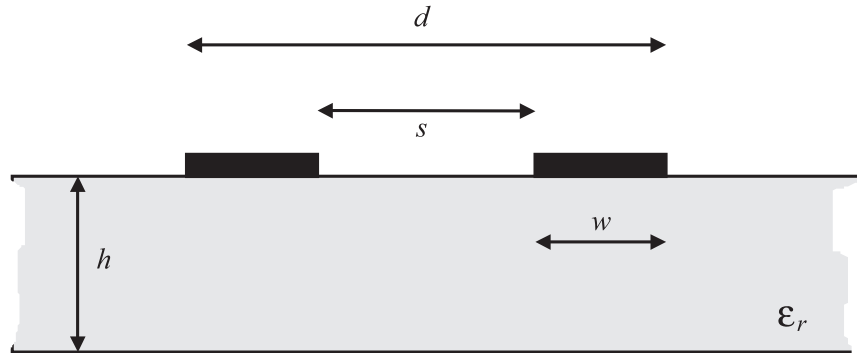

Figure 7. Symmetrical double microstrip line with finite substrate thickness.

For every planar segment the inductance per unit length is known and given by:

$$L_{pl} = \frac{\mu_o h}{W_e} \tag{27}$$

where

$$W_e = \frac{W_{em}(f) + W}{2} \tag{28}$$

with W the physical width of the lines and $W_{em}(f)$, their effective width given by $W_{em}(F) = \frac{\eta_o h}{Z_o(f)\sqrt{\varepsilon_{re}(f)}}$; η_0 the intrinsic wave impedance (120π Ω) of free space; and h the height of the substrate.

From equation (27), the total inductance L_p and mutual inductance M can be calculated as follows:

$$L_p = \frac{L_{11} - \frac{(L_{11}^2 - L_{12}^2)}{L_{pl}}}{1 - 2L_{11}/L_{pl} + \frac{(L_{11}^2 - L_{12}^2)}{L_{pl}^2}} \Delta l \tag{29}$$

and

$$M = \frac{L_{12}}{1 - 2L_{11}/L_{pl} + \frac{(L_{11}^2 - L_{12}^2)}{L_{pl}^2}} \Delta l \tag{30}$$

The above formulation can be easily used for nonsymmetric lines with $L_{11} \neq L_{22}$, which is the case for crosstalk modeling. The complete inductive part of the model is given by a $(2n+4)$ port network [26]. The admittance matrix may be written as follows:

$$[Y_L] = \frac{-j}{\omega(L_p^2 - M^2)}[L_G] \tag{31}$$

The total lumped network required for the modeling is the superposition of capacitive and inductive matrices given by:

$$[Y_G] = [Y_C] + [Y_L] = j\omega[C_G]\frac{j}{\omega(L_p^2 - M^2)}[L_G] \tag{32}$$

where

$$[Y_C] = j\omega[C_G] = j\omega \begin{bmatrix} C_f + C_g & -C_g \\ -C_g & C_f + C_g \end{bmatrix} \tag{33}$$

with $C_g = -C_{12}\Delta l$ and $C_f = (C_e - \frac{\varepsilon_0 \varepsilon_{re} W_e}{h})\Delta l$, C_{12}, C_e, W_e are given by equations (23), (26), and (28), respectively.

For discontinuities and bends the method [28] can be applied by representing the discontinuity with a lumped network (Figure 8). The discontinuity is analyzed into
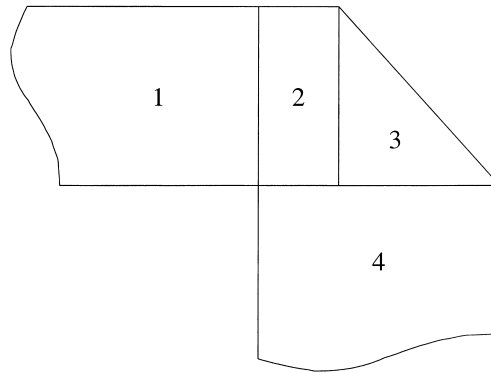
Figure 8. Segmentation of a discontinuity.

elementary segments connected together by a discrete number of interconnections. In this case the above formulation must be used for all contacting segments ($1 \rightarrow 2$, $2 \rightarrow 3$, $3 \rightarrow 4$, $2 \rightarrow 4$). Individual matrices are combined and the overall matrix is calculated. In this way, every discontinuity and bend introducing crosstalk can be easily modeled and calculated.

Table 2
Electrical parameters of a typical wire-bonded OEIC

Electrical parameters	Laser side	Typical calculated values
I1	Laser current	100 mA
L4	Microstrip inductance	0.3 nH
R3	Microstrip resistance	1 ohm
C6	Microstrip capacitance	0.3 pF
L1	Bondwire self-inductance	982 pH
C3	Bondwire capacitance	1 fF
R1	Laser resistance	10 ohm
C2	Laser capacitance	3 nF
L3	Laser inductance	1 pF
	Photodiode side	
R2	Load resistance	10 K
L6	Microstrip inductance	0.3 nH
R4	Microstrip resistance	1 ohm
C6	Microstrip capacitance	0.3 pF
L2	Bondwire self-inductance	982 pH
C4	Bondwire capacitance	1 fF
C1	Photodiode capacitance	5 pF
R6	Photodiode resistance	10 ohm
I2	Photocurrent	~70 nA
	Coupling	
C7	Coupling capacitance	0.04 pF
K	Mutual inductance's coupling coefficient	<0.01

It must be noted that the accuracy of this method is good for discontinuities with lengths of each section on either side greater than twice the width of the lines [28]. This happens in the majority of crosstalk studies in OEICs.

In the same manner, flip-chip circuits can be analyzed and modeled in terms of crosstalk.

The Complete Equivalent Circuit of the OEIC

Using the equivalent circuits of the laser and the photodiode as well as the electrical parameters of each element and their circuitry, the whole OEIC structure can be described by an equivalent circuit. The parameters of this circuit can be calculated using the above-described methods. Such a circuit is useful for the analysis of the module's electrical properties and, in our case, for the estimation of the crosstalk. In Table 2, the electrical parameters used are summarized, and in Figure 9 such circuits for wire-bonded and flip-chip OEICs are presented.

With the above-described equivalent circuit, different cases of placement of the laser and the photodiode can be evaluated in terms of electrical crosstalk behavior. Furthermore, the contribution of each crosstalk source as well as the overall performance of the module can be analyzed and estimated. Besides that, different design aspects can be evaluated and taken into account in the module's design.
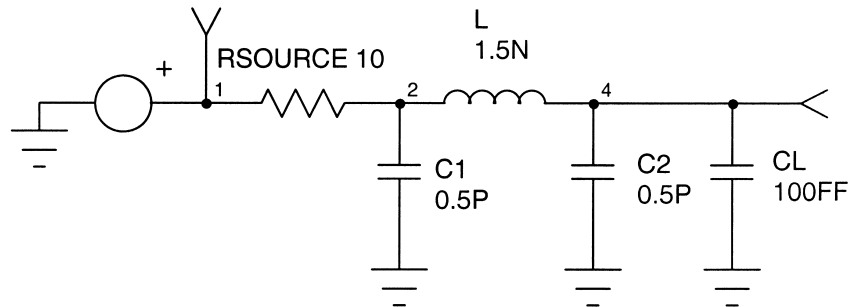

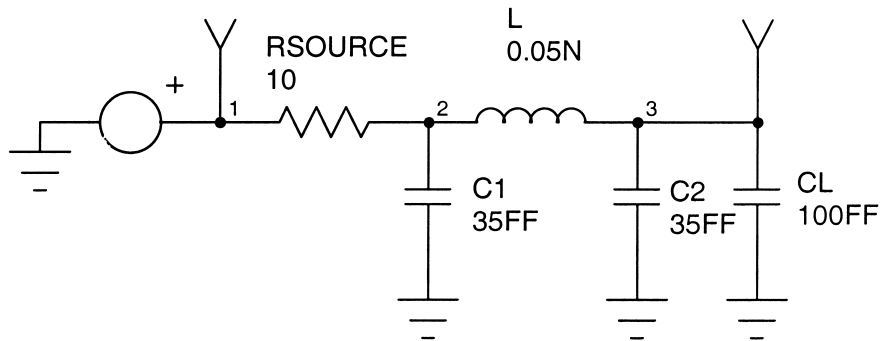**Figure 9a.** Simplified network of a wire-bonded VLSI circuit driving an OE device.

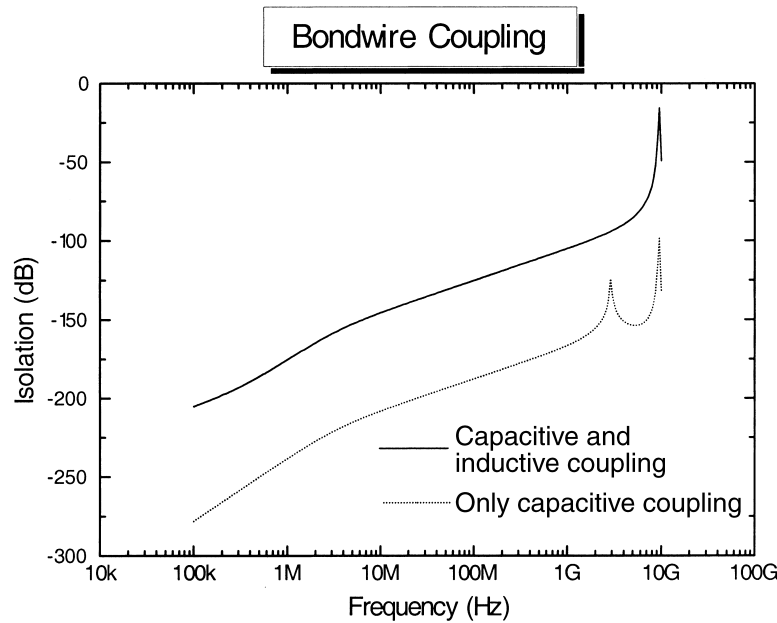**Figure 9b.** Simplified network of a flip-chip VLSI circuit driving an OE device.

Figure 10. The effect of bondwires' mutual inductance to the frequency response of the module.

Results

Inductive vs. Capacitive Coupling

In Figure 10, the contribution of the mutual inductance between the bondwires is presented. The dashed curve is not including the calculation of mutual inductance. In the solid curve this effect has been taken into account and therefore the inductive coupling can be observed. As can be seen, the mutual inductance contributes to the overall crosstalk with up to 40 dB (for parallel bondwires). This effect is crucial for the design of the modules, especially for thin bondwires and high currents. It must be noted that a first resonance frequency at 2.5 GHz (originated from microstrip coupling) is present when inductive coupling has not been taken into account or when bondwires are orthogonally oriented.

Crosstalk Based on Bondwire Orientation

The appropriate design of bondwire orientation can significantly suppress the crosstalk between the laser and the photodiode. In Figure 11, the isolation for different bondwires' orientation is presented. Each pair has two parallel bondwires and the angles represent the orientation of each pair to another. Orthogonally oriented bondwires are in favor of crosstalk suppression. Furthermore, the orientation of bondwires can improve the isolation for more that 30 dBs.

Influence of Amplifier to the Total Crosstalk

In Figure 12, the effect of the load resistance (R2) is presented. The solid curve corresponds to a standard voltage amplifier with 100 kΩ load resistance and the dashed curve
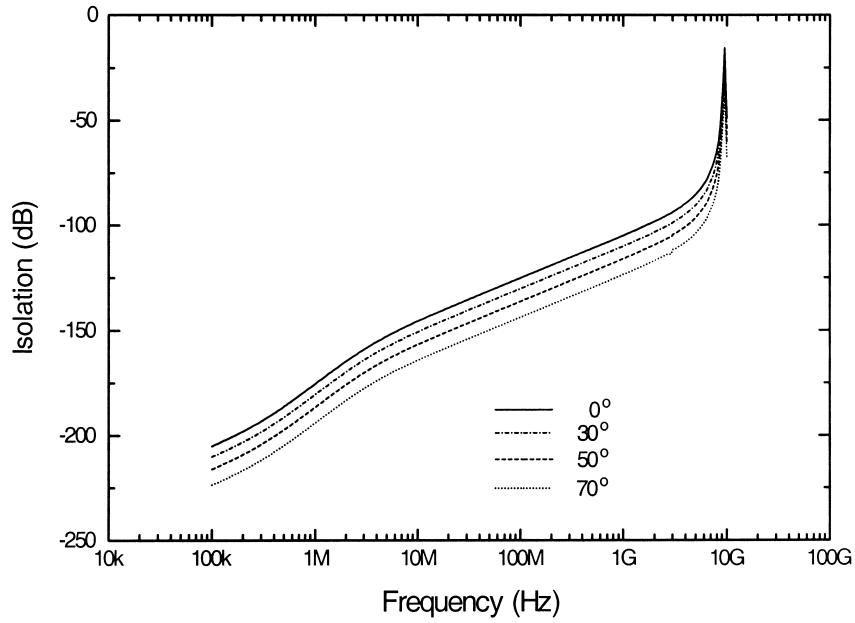
Figure 11. Isolation for different bondwires' angle.

to a transimpedance amplifier with 1 MΩ. It seems that a higher resistance can suppress the effect of the crosstalk or shift it outside the useful bandwidth with appropriate design of the receiver filter. In addition, ringing effects can be suppressed significantly due to appropriate design of the amplifier's resistance (Figure 13).
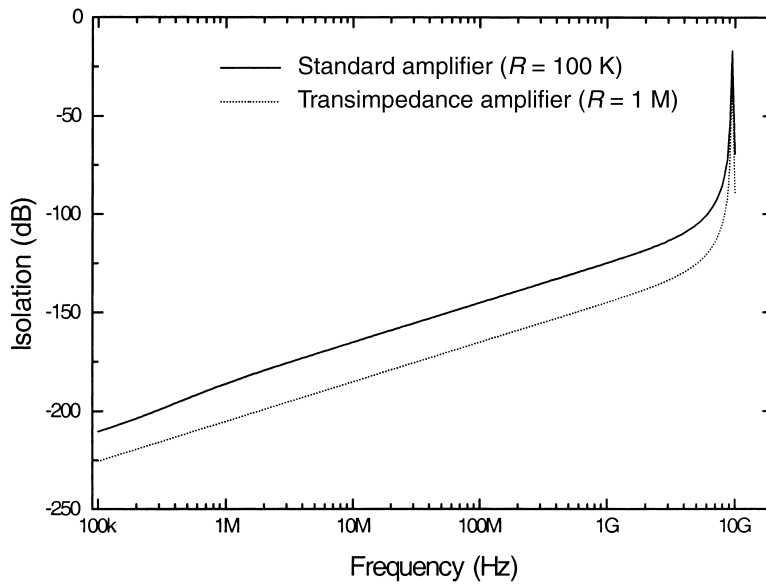

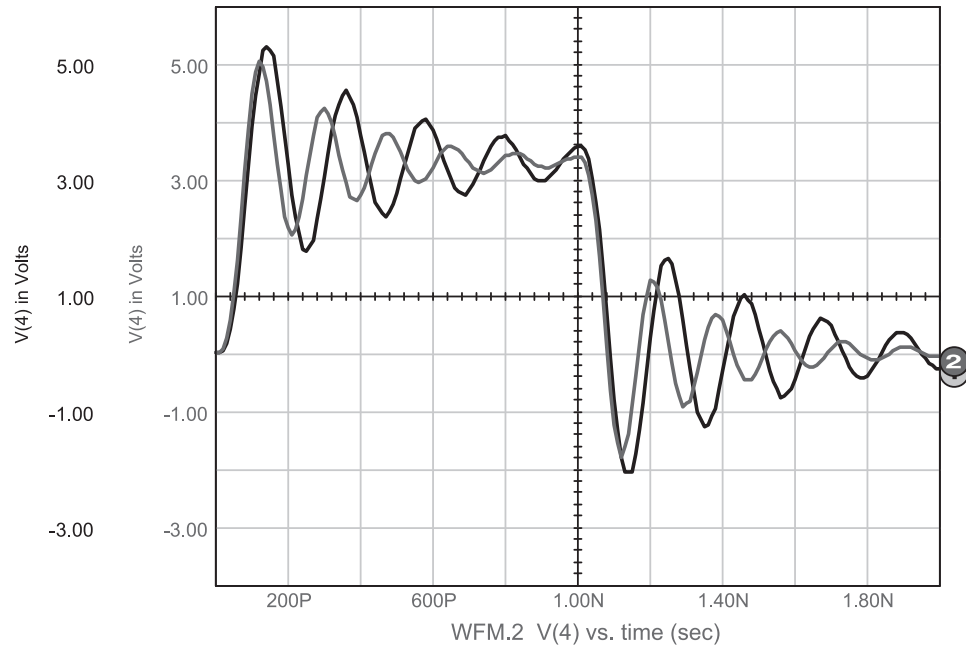**Figure 12.** Crosstalk suppression for differenent types of amplifiers.

Figure 13. Ringing effects for different inductive crosstalk (1 and 1.2 nH) for high-impedance driver.
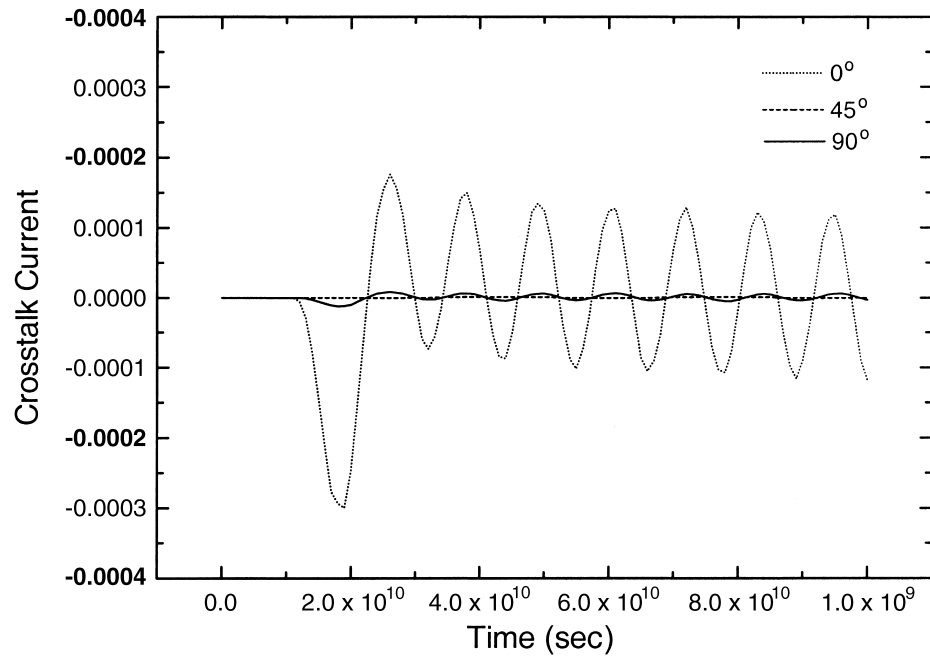

Figure 14. Influence of bondwires' orientation to the current induced at the photodiode.

Transient Analysis

The influence of electrical crosstalk in the time domain is illustrated in Figure 14. Each pair has two parallel bondwires and angles represent the orientation of each pair to another. The parasitic current due to all sources of crosstalk will be added to the current of the photodiode. The orientation of the bondwires, and therefore the inductive crosstalk, is critical for the performance of the module.

Conclusions

In this article, an electrical crosstalk model has been presented taking into account all electrical crosstalk sources. This model allows calculations of the contributions of each crosstalk source. The above-described approach and the results obtained can be summarized in the following conclusions and design tips:

- The crosstalk increases proportionally to the frequency f, especially due to capacitive coupling;
- The inductive crosstalk actually dominates at frequencies above 100 MHz. This is due to the inductive coupling between the bondwires. Thin bondwires should therefore be avoided, especially for high currents, or should be oriented at right angles;
- The appropriate selection of the amplifier's input impedance can significantly suppress the crosstalk;
- Appropriate design of frequency resonance can shift the crosstalk outside the bandwidth of the system.

Moreover, the model can be applied to several OEIC configurations and architectures by calculating the values of electrical parameters and using them in an electrical simulator (e.g., SPICE).

References

1. Khoe, G. D. 2000. Lightwave technology: Expectations, problems and achievements. *IEEE Journal of Selected Topics in Quantum Electronics* 6(6):1265.
2. Kato, K., M. Ishii, and Y. Inoue. 1998. Packaging of large-scale planar lightwave circuits. *IEEE Transactions on Components Packaging, and Manufacturing Technology B* 21:121.
3. Ohyama, T., Y. Akahori, M. Yanagisawa, H. Tsunetsugu, and S. Mino. 1999. Assembly and electrical wiring technologies on planar lightwave circuit (PLC) platform providing hybrid integration of optoelectronic devices and integrated circuits (ICs). *IEICE—Transactions on Communications* E82-B:422.
4. Dagenais, M., R. F. Leheny, H. Temkin, and P. Bhattacharga. 1990. Application and Challenges of OEIC technology: A report on the Hilton Head Workshop. *Journal of Lightwave Technology* 8(6):846.
5. Krishnamoorthy, A. V., and K. W. Goosen. 1998. Optoelectronic-VLSI: Photonics integrated with VLSI circuits. *IEEE Journal of Selected Topics in Quantum Electronics* 4:899.
6. Suzuki, A., K. Kasahara, and M. Shikada. 1987. InGaAsP/InP long wavelength optoelectronic integrated circuits (OEIC's) for high-speed optical fiber communication systems. *Journal of Lightwave Technology* 5(10):1479.
7. Nakano, H., S. Sasaki, M. Maeda, and K. Aiki. 1987. Dual-in-line laser diode module for fiber-optic transmission up to 4 Gbit/s. *Journal of Lightwave Technology* 5(10):1403.
8. Williams, P. J., P. M. Charles, I. Griffiths, N. Carr, D. J. Reid, N. Forbes, and E. Thom. 1994. WDM transceiver OEICs for local access networks. *Electronics Letters* 30(18):1529.

9. Hamacher, M., H. Heidrich, R. Kaiser, P. Albrecht, W. Ebert, S. Malchow, M. Mohrle, W. Rehbein, H. Schroeter-Janßen, and R. Stenzel. 1998. Full-duplex WDM-transceiver-PICs. ECOC'98, Madrid.

10. Foster, G. M., J. R. Rawsthorne, J. P. Hall, M. Q. Kearley, and P. J. Williams. 1995. OEIC WDM transceiver modules for local access networks. *Electronics Letters* 31(2):132.

11. Park, K. S., D. K. Oh, H. M. Kim, and K. E. Pyun. 1998. Compact photonic integrated circuit chip with low crosstalk for bidirectional transceivers. *Electronics Letters* 34(1):79.

12. Nguyen, L. V. T., A. J. Lowery, P. C. R. Gurney, and D. Novak. 1995. A time-domain model for high-speed quantum-well lasers including carrier transport effects. *IEEE Journal of Selected Topics in Quantum Electronics* 1:494.

13. Gao, D. S., S. M. Kang, R. P. Bryan, and J. J. Coleman. 1990. Modelling of quantum-well lasers for computer-aided analysis of optoelectronic integrated circuits. *Journal of Quantum Electronics* 26:1206.

14. Kan, S. C., and K. Y. Lau. 1992. Intrinsic equivalent circuit of quantum-well lasers. *IEEE Photonics Technology Letters* 4:528.

15. Lu, M. F., J. S. Deng, C. Juang, M. J. Jou, and B. J. Lee. 1995. Equivalent circuit model of quantum-well lasers. *IEEE Journal of Quantum Electronics* 31:1418.

16. Tsou, P. C., and D. L. Pulfrey. 1997. A versatile SPICE model for quantum-well lasers. *IEEE Journal of Quantum Electronics* 33(2):246.

17. Sze, S. M. 1981. *Physics of semiconductor devices*. New York: Wiley.

18. Kaplan, D. R., and S. R. Forrest. 1986. Electrical crosstalk in p-I-n arrays, Part I: Theory. *IEEE Journal of Lightwave Technology* 4(10):1460.

19. Smith, S. D. 1995. *Optoelectronic devices*. London: Prentice Hall.

20. Ribeiro, L. 1998. Electrical cross-talk modelling in optoelectronic integrated transceivers. Melecon '98, *9th Mediterranean Electrotechnical Conference*, May 18–20, 1998, Tel-Aviv, Israel.

21. Tsigopoulos, A., A. Chipouras, T. Sphicopoulos, and D. Syvridis. 1997. Electrical crosstalk analysis due to bondwire capacitive induced coupling in OEIC transceiver modules. *International Journal of Optoelectronics* 11(4):239.

22. Harrington, R. F. 1961. *Time harmonic electromagnetic fields*. New York: McGraw Hill.

23. Jansen, R. H. 1978. High speed computation of single coupled microstrips parameters including dispersion, high order modes, loss and finite thickness. *IEEE Transactions on Microwave Theory and Techniques* 26:75.

24. Sabban, A., and K. C. Gupta. 1992. A planar-lumped model for coupled microstrip lines and discontinuities. *IEEE Transactions on Microwave Theory and Techniques* 40(2):245.

25. Hoffman, R. K. 1987. *Handbook of microwave integrated circuits*. Moorwood, MA: Artech House.

26. Sabban, A., and K. C. Gupta. 1991. Characterisation of radiation loss from microstrip discontinuities using a multiport network modeling approach. *IEEE Transactions on Microwave Theory and Techniques* 39(4):705.

Biographies

Dimitris Varoutas holds a physics degree and M.Sc. and Ph.D degrees in electronics and radio communications from the University of Athens. He is a research fellow and adjunct lecturer in the Department of Informatics and Telecommunications of the University of Athens. He is also an adjunct lecturer in the Department of Telecommunications of the newly founded University of Peloponnese. He has participated in numerous European R&D projects in the RACE I and II, ACTS, Telematics, RISI, and IST frameworks in the areas of telecommunications and technoeconomics. He is an advisor in several organizations including OTE and EETT (Greek NRA for telecommunications) in the fields of telecommunications, broadband and mobile services, licensing, spectrum management, pricing, and legislation. His research interests are optical, microwave communications, and technoeconomic evaluation of network architectures and services. He has more than

30 publications in refereed journals and conferences in the area of telecommunications, optoelectronics, and technoeconomics. He is a member of IEEE and serves as reviewer in several journals and conferences.

Angela Arapoyanni received a B.Sc. degree in physics from the University of Athens, Greece, in 1973, M.Sc. degrees in electronics and radioelectrology and electronic automation in 1975 and 1976, respectively, and a Ph.D. in physics in 1983 from the same university. She was an assistant at the Laboratory of Electronic Physics, University of Athens, from 1974 to 1983; a lecturer at the Department of Physics, Division of Applied Physics, University of Athens, from 1983 to 1988, and assistant professor in optoelectronics at the same department from 1988 to 2002. She is currently an associate professor in the Department of Informatics, University of Athens. Since 1979, she has participated in the Optoelectronics Research Group of the University of Athens. Since 1985, she has taught microelectronics to the students of physics and later to the students of Informatics. She is the main author or co-author in more than 65 papers in scientific periodicals and conferences. She received the best paper award of the 2002 International Symposium on Quality Electronic Design. Dr. Arapoyanni is a member of the IEEE.

Thomas Sphicopoulos received a B.Sc. degree in physics from Athens University in 1976, a D.E.A. degree and doctorate in electronics from the University of Paris VI in 1977 and 1980, respectively, and the Doctorat Es Science from the Ecole Polytechnique Federale de Lausanne in 1986. From 1976 to 1977 he worked in Thomson CSF Central Research Laboratories on microwave oscillators. From 1977 to 1980 he was an associate researcher in Thomson CSF Aeronautics Infrastructure Division. In 1980 he joined the Electromagnetism Laboratory of the Ecole Polytechnique Federal de Lausanne where he carried out research on applied electromagnetism. Since 1987 he has been with the Athens University engaged in research on broadband communications systems. In 1990 he was elected as an Assistant Professor of Communications in the Department of Informatics; in 1993 as Associate Professor, and since 1998 he has been a professor in the same department. His main scientific interests are microwave and optical communication systems and networks and technoeconomics. He is leading about 30 national and European R&D projects (RACE I and II, ACTS, RISI, HCM, COST, Eurescom, etc.) including Synthesis and TITAN. He has more than 80 publications in scientific journals and conference proceedings. He is also a reviewer in journals of IEEE and IEE and auditor and evaluator of RACE and ACTS projects. He is the Chairman of the IEEE LEOS Chapter (Bulgaria, Greece, Romania, and Yugoslavia). Since 1999 he advises several organizations including EETT (Greek NRA for telecommunications) in the fields of market liberalization, spectrum management techniques, and technology convergence.